European Journal of Nuclear Medicine and Molecular Imaging (2019) 46:407–420
https://doi.org/10.1007/s00259-018-4179-9

ORIGINAL ARTICLE

Metabotropic glutamate receptor subtype 5 is altered in LPS-induced murine neuroinflammation model and in the brains of AD and ALS patients

Adrienne Müller Herde[1] · Roger Schibli[1] · Markus Weber[2] · Simon M. Ametamey[1]

Received: 23 May 2018 / Accepted: 20 September 2018 / Published online: 5 October 2018

Abstract

Purpose The aim of the present study was to determine the expression levels of mGluR5 in different mouse strains after induction of neuroinflammation by lipopolysaccharide (LPS) challenge and in the brains of patients with Alzheimer's disease (AD) and amyotrophic lateral sclerosis (ALS) post mortem to investigate mGluR5 expression in human neurodegenerative diseases.

Methods C57BL/6 and CD1 mice were injected intraperitoneally with either 10 mg/kg LPS or saline. mGluR5 and TSPO mRNA levels were measured after 1 and 5 days by qPCR, and mGluR5 protein levels were determined by PET imaging with the mGluR5-specific radiotracer [^{18}F]PSS232. mGluR5 expression was evaluated in the post-mortem brain slices from AD and ALS patients using in vitro autoradiography.

Results mGluR5 and TSPO mRNA levels were increased in brains of C57BL/6 and CD1 mice 1 day after LPS treatment and remained significantly increased after 5 days in C57BL/6 mice but not in CD1 mice. Brain PET imaging with [^{18}F]PSS232 confirmed increased mGluR5 levels in the brains of both mouse strains 1 day after LPS treatment. After 5 days, mGluR5 levels in CD1 mice declined to the levels in vehicle-treated mice but remained high in C57BL/6 mice. Autoradiograms revealed a severalfold higher binding of [^{18}F]PSS232 in post-mortem brain slices from AD and ALS patients compared with the binding in control brains.

Conclusion LPS-induced neuroinflammation increased mGluR5 levels in mouse brain and is dependent on the mouse strain and time after LPS treatment. mGluR5 levels were also increased in human AD and ALS brains in vitro. PET imaging of mGluR5 levels could potentially be used to diagnose and monitor therapy outcomes in patients with AD and ALS.

Keywords Metabotropic glutamate receptor subtype 5 · [^{18}F]PSS232 · Positron emission tomography · Neuroinflammation · Neurodegenerative disease · Lipopolysaccharide

Introduction

Neurodegeneration is marked by slow and progressive dysfunction that leads to a loss of neurons and axons in the central nervous system, and is the primary pathological feature of acute and chronic neurodegenerative diseases such as Alzheimer's disease (AD), amyotrophic lateral sclerosis (ALS), Parkinson's disease, Huntington's disease and multiple sclerosis [1]. Despite different triggering events, a common feature is chronic immune activation, in particular of microglia, the resident macrophages of the central nervous system [2]. Brain tissue in patients with neurodegenerative disease is characterized by activation of microglia, marked astrocytosis and measurably elevated levels of inflammatory cytokines. It is well established that peripheral infections accompanied by inflammation are a major risk factor for neuroinflammation and lead to the development of neurodegenerative diseases [3].

A commonly used model is the peripheral injection of lipopolysaccharides (LPS) that represents the current standard paradigm for the study of neuroinflammation both in vivo and

✉ Simon M. Ametamey
simon.ametamey@pharma.ethz.ch

[1] Center for Radiopharmaceutical Sciences of ETH, PSI, and USZ, Department of Chemistry and Applied Biosciences of ETH, 8093 Zurich, Switzerland

[2] Neuromuscular Diseases Unit/ALS Clinic, Kantonsspital St. Gallen, 9007 St. Gallen, Switzerland

in vitro [4]. The endotoxin of gram-negative bacterial cell walls contains LPS as its principal inflammatory constituent. LPS induces a variety of central effects mediated by proinflammatory cytokines released mainly from microglia [5]. Although it is accepted that cytokines released in the periphery do not diffuse across the blood–brain barrier (BBB), they may transfer their signal to the brain. Numerous studies in animals, especially mice and rats, have demonstrated that LPS is able to stimulate from the periphery the synthesis of proinflammatory cytokines in the brain [6]. During an inflammatory response in the brain, activation of microglia leads to retraction of their processes and swelling of their cell bodies. This in turn may induce neuronal damage, disruption of relevant circuits, chronic neuroinflammation and functional decline. Under normal conditions, very little peripheral LPS enters the brain due to poor passage through the BBB [7]. Thus, LPS-induced neuroinflammation is probably an indirect effect.

In an effort to understand how inflammation is transferred from the periphery to the brain, Qin et al. administered TNFα peripherally to mice and found that both TNFα and LPS administration increased the expression of brain proinflammatory factors (e.g. TNFα, MCP-1, IL-1β) in a similar pattern [8]. Numerous other studies in mice with LPS have shown increases in the numbers of cells with F4/80, CD11, CD45 or Iba-1 positivity and morphological changes of microglia after a single or multiple peripheral treatments [8–10]. An increase in the expression of translocator protein (TSPO; also known as peripheral benzodiazepine receptor, PBR), which is present on the mitochondria of activated microglia, astroglia and macrophages, is also associated with neuroinflammation [11]. This supports the premise that inflammation is both an initiating stimulus and a self-perpetuating mechanism of progressive neurodegeneration.

As well as the excessive amount of inflammatory cytokines, it is also well known that neurotransmitters such as glutamate are abundantly present [12]. They lead to excitotoxicity and cell death in response to the activation of glutamate receptors as reported in several pathologies including the above neurodegenerative diseases. The widely distributed metabotropic glutamate receptor subtype 5 (mGluR5) plays a role in many critical neuronal processes including synapse formation [13], long-term depression, glial–neuronal interaction and neuroinflammation [14]. mGluR5 is a seven transmembrane spanning G protein-coupled receptor located in the postsynaptic membrane of excitatory synapses [15] in neuronal cell membranes [16] and in non-neuronal cells such as glial cells [17] and oligodendrocytes [18]. In vivo, a link between inflammation and mGluR5 modulation has been found, especially under pathological conditions such as neuropathic pain, ALS, epilepsy, and multiple sclerosis [12].

The aim of this study was to elucidate the effects of systemic LPS exposure on the availability of mGluR5 in the mouse brain. We used our mGluR5-specific radiotracer [^{18}F]PSS232 [19] to follow mGluR5 expression using in vivo positron emission tomography (PET). Due to the reported different susceptibilities of mouse strains to LPS challenge, we used two different mouse strains, that is the inbred strain C57BL/6 and the outbred strain CD1. Another important point to consider when measuring neuroinflammatory effects is the time after LPS administration. We chose two different time points after LPS challenge to investigate the changes in mGluR5 expression. To highlight the importance of mGluR5 in neurodegenerative diseases and also to show the clinical relevance of mGluR5 imaging, we performed autoradiography studies on brain tissues from AD and ALS patients post mortem and compared them to control samples.

Materials and methods

Animals

The animal studies were approved by the Veterinary Office of Canton Zurich, Switzerland, and carried out according to the 'Guide to the Care and Use of Experimental Animals' of Swiss legislation on animal welfare. Male C57BL/6NCrl and Crl:CD1(ICR) mice at 8 weeks of age were purchased from Charles River (Sulzfeld, Germany). Their body weights at the time of the experiments were between 22 and 27 g. They were kept in a temperature-controlled room (21 °C) under a 12-h light/12-h dark cycle with access to food and water ad libitum.

Drug treatment

Mice received a single intraperitoneal injection of 10 mg/kg LPS (strain *E. coli* 055:B5, L2880; Sigma, St. Louis, MO, USA) or vehicle (0.9% NaCl solution). For quantitative RT-PCR, mice were killed without any treatment (reference, $n = 3$), 1 day after vehicle injection ($n = 3$) or LPS injection ($n = 3$), and 5 days after vehicle injection ($n = 3$) or LPS injection ($n = 3$). PET scans were performed 20–24 h (referred to as 1 day) after vehicle injection ($n = 4$) or LPS ($n = 4$) injection, and 5 days after vehicle injection ($n = 4$) or LPS injection ($n = 4$).

Quantitative reverse transcription-polymerase chain reaction (qRT-PCR)

For total RNA isolation mouse whole brains were disrupted and homogenized using the Isol-RNA lysis reagent (5 PRIME, Gaithersburg, MD, USA) and the bead-milling TissueLyser system (Qiagen, Hilden, Germany). RNA clean-up was performed using on-column DNase digestion with the RNase-free DNase set (Qiagen). The purity and concentration of the extracted total RNA were tested using a

NanoDrop 1000 spectrometer (Thermo Fisher Scientific, Runcorn, UK). QuantiTect® reverse transcription kit (Qiagen) was used to generate cDNA. The qPCR analysis of selected genes was performed with the DyNAmo Flash SYBR® Green qPCR kit (Thermo Fisher Scientific) using a 7900 HT fast real-time PCR system (Applied Biosystems, Carlsbad, CA, USA). Mouse primer sequences were as follows: mouse β-actin (*Actb*) forward 5′-AGAC CTCTATGCCAACACAGT-3′, reverse 5′-TGCT AGGAGCCAGAGCAGTAA-3′; mouse mGluR5 (*Grm5*) forward 5′-TGTAACTCAAGACCTGAATCTATGG-3′, reverse 5′-GCTGGGCCAACTGAACTTTA-3′; mouse translocator protein (*TSPO*) forward 5′-ACTG TATTCAGCCATGGGGTA-3′, reverse forward 5′-ACCA TAGCGTCCTCTGTGAAA-3′. Primers were custom-made oligonucleotides synthesized by Microsynth (Balgach, Switzerland). All reactions were performed in duplicate and in at least two independent runs. Gene expression data were analysed by normalization against the housekeeping gene β-actin and quantified by the $2^{-\Delta\Delta Ct}$ method. The specificity of the PCR products of each run was determined and verified using the SDS dissociation curve analysis feature.

In vivo PET/CT imaging

In vivo PET imaging was performed using [^{18}F]PSS232 which was first evaluated by our group [19]. In vivo PET/CT scans were performed using a calibrated Super Argus scanner (Sedecal, Madrid, Spain). Mice were anaesthetized with isoflurane (Isocare; Animalcare, York, UK) at a concentration of 2% in a 1:1 mixture of oxygen and air and a flow rate of 0.4 L/min. The total duration of anaesthesia was 75 min (10 min for induction and placing the animal on the scanner bed, 60 min PET scan, 5 min CT acquisition). The total duration of anaesthesia was kept similar and was not changed between animals or groups. The respiratory rate and body temperature were controlled during the whole scan period (SA Instruments, Inc., Stony Brook, NY, USA). Mice were placed in a prone position and the brain was positioned in the centre of the field of view. The radioligand was administered by injection into a tail vein. For blocking experiments, the mGluR5 antagonist 2-((3-methoxy-phenyl)ethynyl)-6-methylpyridine (MMPEP) was dissolved in a 1:1 solution of PEG200 in water for injection, and 1 mg/kg was administered intravenously 10 s before the radiotracer. PET acquisition was started 1 min after radiotracer injection, was continued for 60 min and was followed by a CT scan. Mice were imaged only once and were killed at the end of a single PET/CT scan. Table 1 presents the body weights, injection parameters and the start times of the PET scan in each group. Significant differences between groups were found for body weight and injected radioactivity.

Image reconstruction, analysis and calculation of distribution volume ratios

PET data were reconstructed in user-defined time frames (5 × 2 min, 2 × 5 min, 1 × 10 min, 2 × 15 min) with a voxel size of 0.3875 × 0.3875 × 0.775 mm using a two-dimensional ordered subsets expectation maximization (2D-OSEM) algorithm. Random and single correction were applied but no attenuation correction. Image files were analysed with PMOD 3.6 software (PMOD Technologies Ltd., Zurich, Switzerland). PET images were manually matched to the corresponding CT images, and in a next step the CT images were manually matched to the rat MRI T2 template (provided with PMOD software). The resulting transformations were applied to the PET images to obtain PET images matched to the MRI T2 template. Brain regions of interest including the striatum, hippocampus, cortex, thalamus, midbrain, whole brain and cerebellum were defined based on the rat MRI T2 template. Standardized uptake values (SUV) were calculated from the image-derived radioactivity in becquerels per cubic centimetre of tissue divided by the radioactivity dose in becquerels per gram body weight, assuming a tissue density of 1 g/cm^3. SUVs were plotted as time–activity curves (TACs) for the striatum and cerebellum. Given that hardly any specific binding was found in the cerebellum of the mice, this brain region was used as the reference region. Distribution volume ratios (DVRs) were calculated from the areas under the curve (AUCs) as described recently [20].

Post-mortem human brain tissue

Frozen post-mortem human brain tissue blocks from patients with late stage ALS ($n = 3$) and corresponding healthy controls ($n = 2$) were provided with the written consent of the donors by the Cantonal Hospital St. Gallen, Switzerland. The University Hospital Alcorcón, Spain and the Victorian Brain Bank Network, The University of Melbourne, Australia, provided frozen post-mortem human brain tissue from patients with severe AD (Alcorcón $n = 2$, Melbourne $n = 4$) and corresponding healthy controls (Alcorcón $n = 2$; Melbourne $n = 4$) with the written consent of the donors.

In vitro autoradiography

In vitro autoradiography with [^{18}F]PSS232 was performed on 10-μm cryosections of human post-mortem ALS and AD brains. Sections were thawed on ice for 10 min before preincubation with incubation buffer (30 mM HEPES, 1.2 mM $MgCl_2$, 110 mM NaCl, 2.5 mM $CaCl_2$, 5 mM KCl, pH 7.4, in 0.1% BSA) at 4 °C for another 10 min. Excess solution was carefully removed and the slides were incubated with 1 nM [^{18}F]PSS232 alone or together with mGluR5

Table 1 Body weights, [^{18}F]PSS232 injection data and start times of the PET scan in each animal group together with the significance of differences between groups

Strain	Days after treatment	Treatment	MMPEP blocking	Number of animals	Body weight on day of scan (g)	Injected radioactivity at scan start (MBq)	Injected molar radioactivity at scan start (GBq/μmol)	Injected dose at scan start (nmol/kg)	Time at scan start
C57BL/6	1 day	Vehicle	No	4	24.9 ± 1.3	10.2 ± 0.6	81.4 ± 57.2	12.9 ± 12.8	11.30 a.m. to 3.30 p.m.
		Vehicle	Yes	4	25.3 ± 2.4	11.1 ± 0.4	59.1 ± 25.0	8.5 ± 2.7	1.00 p.m. to 2.00 p.m.
		LPS	No	4	22.4 ± 0.9	10.6 ± 0.5	62.5 ± 25.7	9.9 ± 5.9	1.00 p.m. to 2.30 p.m.
		LPS	Yes	4	22.4 ± 1.5	11.4 ± 0.4	71.6 ± 55.9	11.4 ± 6.4	11.30 a.m. to 3.30 p.m.
	5 days	Vehicle	No	4	26.5 ± 1.5	9.3 ± 1.3	57.0 ± 60.4	14.4 ± 12.7	12.00 p.m. to 5.00 p.m.
		Vehicle	Yes	4	25.3 ± 1.4	11.3 ± 1.3	51.6 ± 8.4	8.8 ± 0.5	2.00 p.m. to 3.00 p.m.
		LPS	No	4	24.0 ± 2.1	9.5 ± 1.6	55.3 ± 34.6	17.8 ± 19.6	1.00 p.m. to 6.30 p.m.
		LPS	Yes	4	23.8 ± 0.8	11.9 ± 0.8	25.9 ± 8.2	21.1 ± 5.1	3.30 p.m. to 4.30 p.m.
CD1	1 day	Vehicle	No	4	29.1 ± 1.1	10.0 ± 2.3	73.2 ± 47.5	7.8 ± 4.8	11.30 a.m. to 5.00 p.m.
		Vehicle	Yes	4	29.5 ± 1.8	9.3 ± 2.3	24.3 ± 12.0	14.8 ± 4.5	2.00 p.m. to 4.00 p.m.
		LPS	No	4	26.6 ± 1.9	9.5 ± 1.2	54.9 ± 23.2	7.9 ± 4.1	1.00 p.m. to 3.00 p.m.
		LPS	Yes	4	25.9 ± 1.4	6.1 ± 2.2	23.6 ± 12.3	12.7 ± 5.5	1.00 p.m. to 3.00 p.m.
	5 days	Vehicle	No	4	30.0 ± 2.4	13.4 ± 1.2	61.7 ± 35.5	13.9 ± 12.4	11.00 a.m. to 5.00 p.m.
		Vehicle	Yes	4	31.1 ± 5.3	12.2 ± 0.7	59.8 ± 41.5	9.7 ± 5.3	11.30 a.m. to 2.00 p.m.
		LPS	No	4	29.3 ± 3.6	12.3 ± 0.6	47.8 ± 25.9	16.3 ± 15.3	12.30 a.m. to 6.00 p.m.
		LPS	Yes	4	29.1 ± 4.2	12.7 ± 1.4	24.6 ± 7.1	19.5 ± 5.9	2.30 p.m. to 3.30 p.m.
Between-group analysis		$F_{(15,48)}$			5.862	5.954	0.9264	0.7395	0.5274
		p value			<0.0001	<0.0001	0.5423	0.7330	0.9123

antagonist MMPEP (1 μM final concentration) in incubation buffer. After incubation for 40 min at room temperature in a wet chamber, the slides were washed in ice-cold incubation buffer for 5 min and twice in washing buffer (30 mM HEPES, 1.2 mM $MgCl_2$, 110 mM NaCl, 2.5 mM $CaCl_2$, 5 mM KCl, pH 7.4) for 2 min each and dipped twice in distilled water. Dried slides were exposed to a phosphor imager plate (BAS-MS 2025; Fuji, Dielsdorf, Switzerland) for 10 min and the plate was scanned in a BAS-5000 reader (Fuji). Finally, all sections were stained with haematoxylin (Gill No. 1; Sigma) and eosin (Eosin Y; Sigma) according to the manufacturer's protocols. All stained sections were digitized using a slide scanner (Pannoramic 250; Sysmex, Horgen, Switzerland) and analysed using Pannoramic Viewer software. For ALS brain tissue, three experiments were conducted independently with two brain slices in each experiment, resulting in six data points. For AD brain tissue, two experiments were conducted independently with two brain slices in each experiment, resulting in four data points. The number of photostimulated luminescence events per square millimetre (mean ± SD) corrected for the size of the tissue was subtracted from the accumulated radioactivity under blocking conditions (MMPEP) to calculate the specific binding.

Statistical analysis

Average values are shown as arithmetic means with standard deviations (SD) or standard errors (SE). Data were evaluated using GraphPad Prism version 7 (GraphPad, La Jolla, CA, USA). The distribution of grouped values was tested for normality using the D'Agostino-Pearson omnibus test. For gene expression data, intergroup significance was tested using one-way ANOVA with Holm-Sidak's multiple comparisons test.

In each animal, TSPO and mGluR5 mRNA expression levels were measured. TSPO and mGluR5 levels in the same animal were correlated and plotted as single data points (three animals per group, four groups). Regression functions including R^2 were calculated including all 12 data points. The normality test revealed normal distributions. Parametric analysis was conducted and Pearson's r calculated.

The significances of differences in DVR between brain regions within subjects and between groups (vehicle vs. LPS) were tested uisng two-way ANOVA with Tukey's multicomparison test. For group parameters (see Table 1) and in vitro autoradiography analysis, the significance of intergroup differences was tested using one-way ANOVA with Tukey's multicomparison test. A p value <0.005 was considered significant.

Results

mGluR5 and TSPO activation to systemic LPS administration

To understand the effects of systemic LPS on brain inflammation, we administered a single peripheral dose of LPS (10 mg/kg) to male C57BL/6 or CD1 mice. TSPO, which is primarily localized on glial cells, is associated with the inflammatory response and neurodegenerative diseases [21]. In order to confirm the inflammatory response in the mouse brains in our experimental setup, we measured TSPO mRNA expression after LPS or vehicle administration.

In C57BL/6 mice, TSPO mRNA expression was increased 3.6-fold ($p < 0.0001$) 1 day after LPS administration and was increased 2.3-fold ($p < 0.0001$) at 5 days (Fig. 1a). There were statistically significant differences among all groups (reference, vehicle at 1 and 5 days, and LPS at 1 and 5 days; $F_{(4,35)} = 123.3$, $p < 0.0001$). In CD1 mice, TSPO mRNA expression was increased 2.6-fold ($p < 0.0001$) 1 day after LPS administration and decreased to a 1.5-fold increase ($p < 0.0001$) at 5 days (Fig. 1b). There were statistically significant differences among all groups (reference, vehicle at 1 and 5 days, and LPS at 1 and 5 days; $F_{(4,35)} = 109.3$, $p < 0.0001$). In C57BL/6 mice, mGluR5 mRNA expression was increased 3.4-fold ($p < 0.001$) 1 day after LPS administration and decreased to a 1.9-fold increase ($p < 0.001$) at 5 days (Fig. 1c). There were statistically significant differences among all groups (reference, vehicle at 1 and 5 days, and LPS at 1 and 5 days; $F_{(4, 35)} = 35.69$, $p < 0.0001$). In CD1 mice, mGluR5 mRNA expression increased 1.9-fold ($p < 0.001$) 1 day after LPS administration, but decreased to a 1.3-fold increase ($p = 0.052$) after 5 days (Fig. 1d). There were statistically significant differences among all groups (reference, vehicle at 1 and 5 days, and LPS at 1 and 5 days; $F_{(4, 35)} = 36.73$, $p < 0.0001$).

mGluR5 expression was positively associated with TSPO expression in both mouse strains (Fig. 1e, f). Low TSPO levels, e.g. in the vehicle-treated groups, were correlated with low mGluR5 levels and vice versa. In the C57BL/6 mice, the regression equation was $y = 0.87x - 0.0242$ ($R^2 = 0.7205$, Pearson's $r = 0.8488$). The slope of the regression line was significantly non-zero ($F_{(1,10)} = 25.78$, $p = 0.0005$). In the CD1 mice, the regression equation was $y = 0.5466x + 0.517$ ($R^2 = 0.9145$, Pearson's $r = 0.9563$). The slope of the regression line was significantly non-zero ($F_{(1,10)} = 107$, $p < 0.0001$).

Regional mGluR5 activation in the mouse brain

Figure 2 shows the TACs of [^{18}F]PSS232 in mGluR5-rich striatum and cerebellum, which shows negligible mGluR5

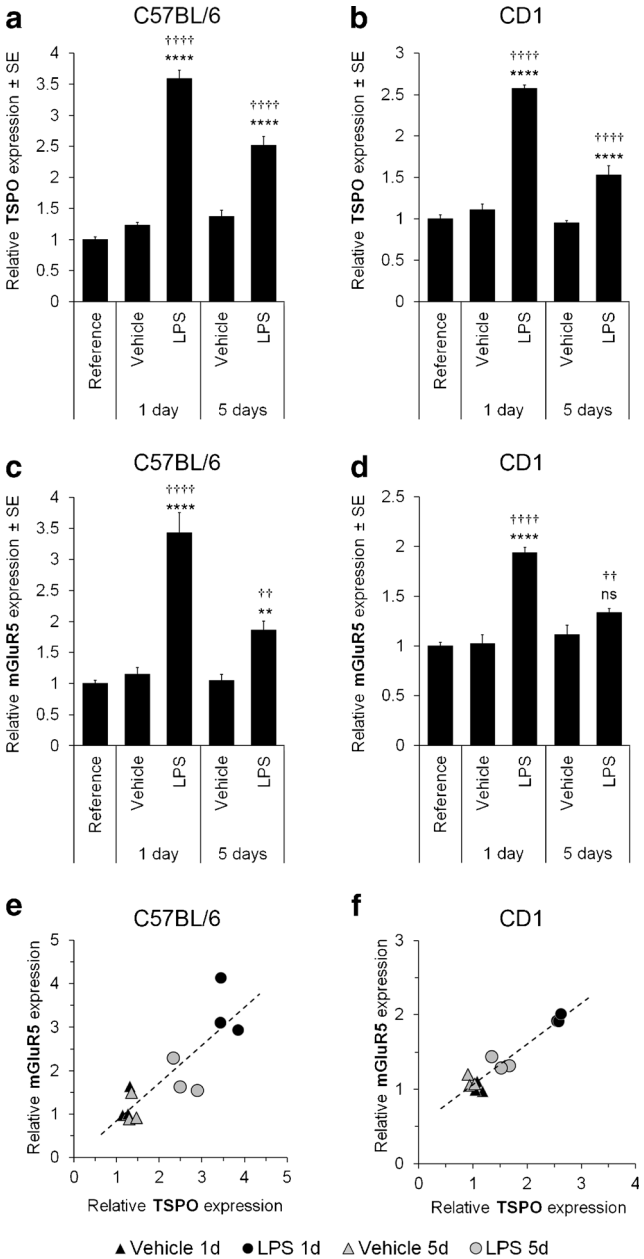

Fig. 1 Effect of systemic LPS administration on TSPO (**a**, **b**) and mGluR5 (**c**, **d**) mRNA expression in the brain of C57BL/6 (**a**, **c**) and CD1 (**b**, **d**) mice at 1 and 5 days after treatment. TSPO and mGluR5 mRNA expression was detected by qRT-PCR and is expressed relative to the reference (untreated mouse brain). Bars represent average values ± standard error (SE). Three animals were used per condition. $^{\dagger\dagger}p < 0.005$ and $^{\dagger\dagger\dagger\dagger}p < 0.0001$ versus reference; $^{**}p < 0.005$ and $^{****}p < 0.0001$ versus vehicle-treated group for the same day. **e**, **f** Correlations between relative TSPO with mGluR5 mRNA expression in C57BL/6 (**e**) and CD1 (**f**) mice. Each data point represents one animal. The dashed lines are the regression lines

levels, 1 and 5 days after LPS or vehicle administration. In C57BL/6 and CD1 mice, striatal binding of [^{18}F]PSS232 was higher in the LPS-treated than in the vehicle-treated mice at both time points with the exception of CD1 mice 5 days after LPS administration (Fig. 2). The striatal TACs in the CD1 mice 5 days after LPS administration were similar to those in the vehicle-treated mice. Administration of the mGluR5 antagonist MMPEP abolished striatal [^{18}F]PSS232 binding in vehicle-treated and LPS-treated mice. The cerebellum showed low [^{18}F]PSS232 binding after vehicle and LPS treatment.

DVRs (as a measure of mGluR5 density) were calculated to compare the effects of LPS treatment in selected brain regions in C57BL/6 and CD1 mice (Fig. 3). Compared with vehicle treatment, LPS treatment led to significantly higher mGluR5 availability 1 day after administration in the striatum (22%, $p < 0.0001$, and 21%, $p < 0.0001$, in C57BL/6 and CD1 mice, respectively), hippocampus (24%, $p < 0.0001$, and 20%, $p < 0.0001$, respectively), cortex (17%, $p = 0.0004$, and 19%, $p < 0.0001$, respectively) and whole brain (16%, $p = 0.0043$, and 13%, $p = 0.0037$, respectively) . mGluR5 availability in the thalamus was significantly higher only in CD1 mice (13%, $p = 0.0053$). A significant effect between brain regions within subjects was found in C57BL/6 mice ($F_{(6,42)} = 191.8$, $p < 0.0001$) and in CD1 mice ($F_{(6,35)} = 364.1$, $p < 0.0001$).

At 5 days, mGluR5 DVRs remained higher in LPS-treated than in vehicle-treated C57BL/6 mice, except for the whole brain. DVR values in C57BL/6 mice 5 days after LPS administration were significantly increased in the striatum (17%, $p < 0.0001$), hippocampus (19%, $p < 0.0001$) and cortex (12%, $p = 0.0186$). On day 5, DVRs of the LPS-treated CD1 mice had decreased to the levels in the vehicle-treated mice. ANOVA showed a significant effect between brain regions within subjects in C57BL/6 mice ($F_{(6,42)} = 210.6$, $p < 0.0001$) and CD1 mice ($F_{(6,35)} = 55.25$, $p < 0.0001$).

To corroborate the region-wise findings, the average voxel-wise DVR within each group was calculated and the results plotted as DVR brain maps (Fig. 4). The PET images clearly demonstrated an increase in DVR 1 day after LPS challenge in both mouse strains. However, at 5 days after LPS administration only C57BL/6 mice showed an increase in DVR values.

Regional mGluR5 activation in the brain of ALS and AD patients

To determine if mGluR5 availability is altered in neurodegenerative diseases, in which neuroinflammation has been implicated, we examined brain slices from ALS and AD patients post mortem using in vitro autoradiography. [^{18}F]PSS232 binding was higher in late stage ALS brains than in non-ALS control brains (Fig. 5). High mGluR5 availability was seen in the motor cortex (3.3-fold, $p < 0.0001$), frontal cortex (2.5-fold, $p < 0.0001$) and temporal cortex (4.2-fold, $p < 0.0001$). The same was observed in the basal ganglia with 3.0-fold higher [^{18}F]PSS232 binding in all ALS brains ($p < 0.0001$). ANOVA showed a nonsignificant effect between experiments (test–retest; $F_{(2,38)} = 0.6556$, $p = 0.5249$).

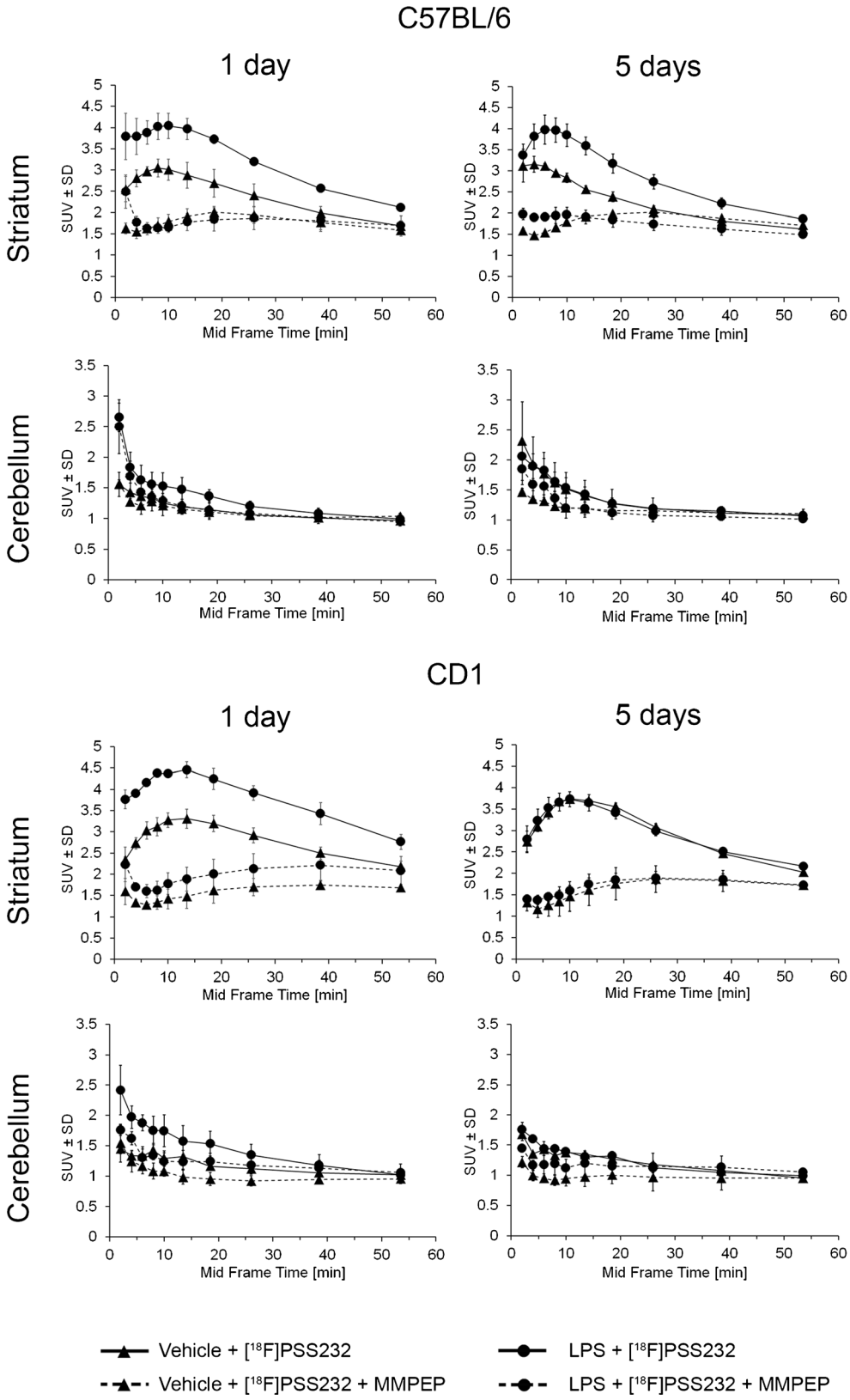

Fig. 2 Time–activity curves for [^{18}F]PSS232 in the striatum (mGluR5-positive) and cerebellum (mGluR5-negative) in C57BL/6 and CD1 mice treated with vehicle (*triangles*) or LPS (*circles*). PET scans were performed 1 and 5 days after vehicle or LPS administration. Blocking experiments were performed with 1 mg/kg MMPEP injected shortly before the radiotracer. The data points represent the mean standardized uptake values ± standard deviation (four animals per group)

Coincubation with MMPEP reduced [^{18}F]PSS232 binding in non-ALS and ALS brains.

Autoradiography on brain slices from AD patients and healthy controls post mortem further demonstrated increased

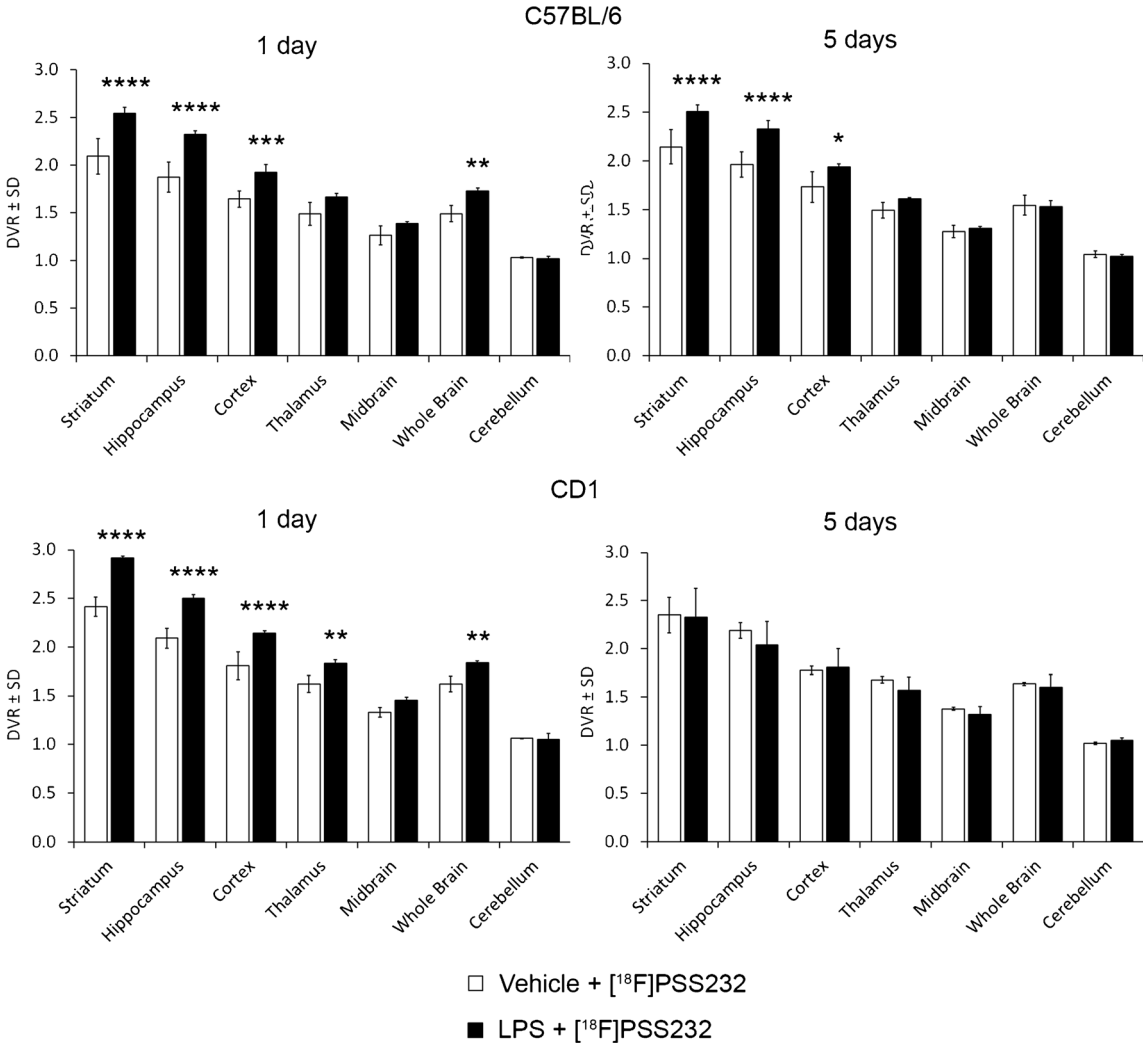

Fig. 3 Influence of systemic LPS treatment on mGluR5 distribution volume ratios (DVRs) in different brain regions in C57BL/6 and CD1 mice 1 and 5 days after treatment. The bars represent mean DVRs ± standard deviation (four animals per group). *$p < 0.005$, **$p < 0.001$, ***$p < 0.0005$, ****$p < 0.0001$, versus vehicle-treated group

[^{18}F]PSS232 binding in the frontal cortex (5.2-fold, $p < 0.0001$) and hippocampus (2.5-fold, $p < 0.0001$) in brains from patients with severe disease compared with brains from healthy controls (Fig. 6). Less [^{18}F]PSS232 binding in the cerebellum was expected due to low densities of mGluR5 in this brain region in healthy controls [22]. mGluR5 availability was not significantly different in the cerebellum of AD patients as [^{18}F]PSS232 binding was marginally higher (1.2-fold, $p = 0.9266$) than in controls. ANOVA showed a nonsignificant effect between experiments (test–retest; $F_{(1,5)} = 0.0291$, $p = 0.8713$).

Discussion

It has been shown that expression of mGluR5 is not limited to neuronal cells, and is profusely increased in glial cells activated by the inflammatory stimulus from LPS [14, 23]. Glial mGluR5 activation plays a role in triggering communication between neurons and glial cells [24]. In this context, astrocytic mGluR5 activation generates sustained calcium oscillations inside reactive astrocytes which triggers the release of stored intracellular glutamate, thus enhancing the neuronal excitability leading to excitotoxicity followed by neuronal loss. Microglial mGluR5 activation causes release of proinflammatory cytokines (IL-6, TNFα, INFγ) leading to progressive neuroinflammation. In neurons and glial cells, mGluR5-mediated signal transduction involves activation of phospholipase C and protein kinase C (PKC), increased inositol trisphosphate, and the release of intracellular calcium [25]. Both diacylglycerol and calcium are able to activate PKC, which has a multitude of actions within the cell, including activation of transcription factors and alteration of potassium channel activity [26, 27], which in turn may adjust glial responses. The resulting pathophysiological impairments of glial mGluR5 are associated with the development of

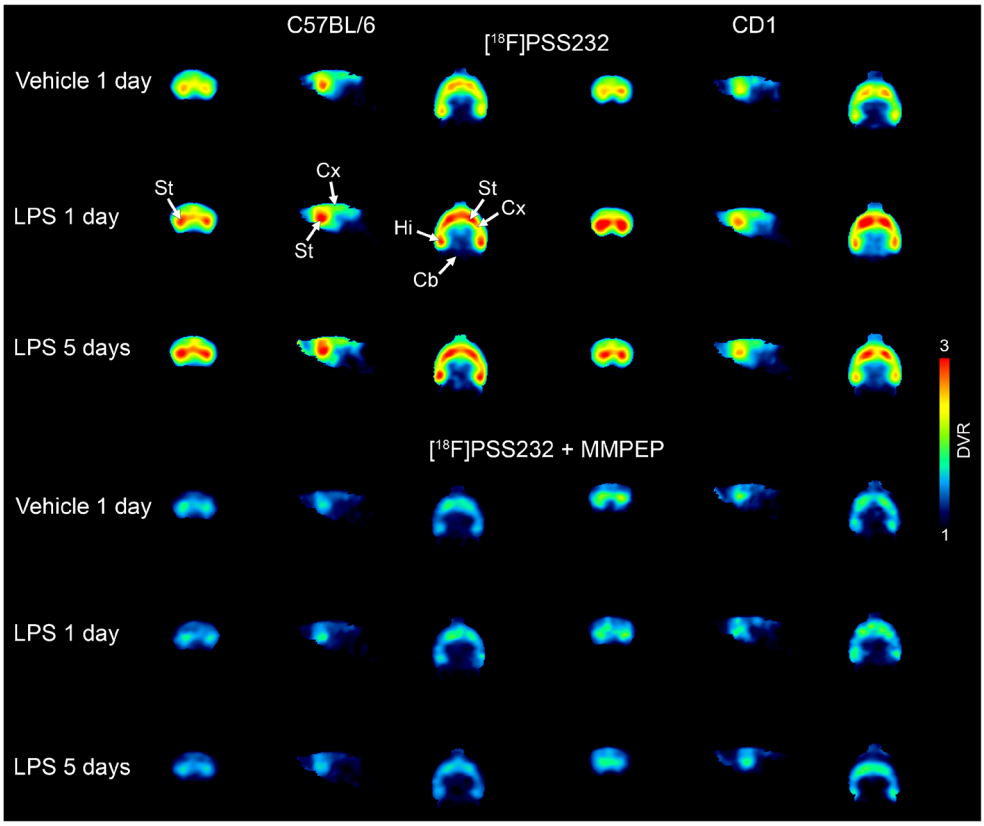

Fig. 4 Brain PET images of [^{18}F]PSS232 as distribution volume ratios (DVR) in C57BL/6 and CD1 mice 1 day after vehicle treatment and 1 and 5 days after LPS treatment. Axial, sagittal and coronal DVR images are shown. The highest accumulation of [^{18}F]PSS232 is seen in the striatum, hippocampus and cortex, particularly after LPS treatment, and low [^{18}F]PSS232 binding in the cerebellum (*St* striatum, *Hi* hippocampus, *Cx* cortex, *Cb* cerebellum). [^{18}F]PSS232 accumulation is abolished by injection of the mGluR5 antagonist MMPEP (1 mg/kg)

neurodegenerative diseases [21]. The underlying mechanism is related to decreased glutamate reuptake and suppression of mGluR5-dependent glial loss. Many of the observations were made with allosteric modulators including MTEP (3-((2-methyl-4-thiazolyl)ethynyl)pyridine), MPEP (2-methyl-6-(phenylethynyl)pyridine) and CDPPB (3-cyano-*N*-(1,3-diphenyl-1*H*-pyrazol-5-yl)benzamide) [28]. These observations suggest the role of mGluR5 in certain physiological as well as pathological events along with other receptors, such as NMDA receptors and ionotropic glutamate receptors.

The present study showed significant changes in mGluR5 availability in an LPS-induced animal model of neuroinflammation. Following a single 10 mg/kg peripheral dose of LPS to mice, [^{18}F]PSS232 uptake increased by approximately 17–24% depending on the brain region, with the highest increases in the striatum, hippocampus and cortex, brain regions known to express high levels of mGluR5. mGluR5 availability increased 1 day after LPS administration in both mouse strains, C57BL/6 (inbred) and CD1 (outbred). Whereas mGluR5 availability remained high until 5 days after LPS administration in the C57BL/6 strain, it declined to control levels in the CD1 strain. An important point to consider when using this neuroinflammation model is the mouse strain. We observed, at least for mGluR5 and TSPO, different regulation in the inbred and outbred strains with longer-lasting mGluR5 and TSPO mRNA levels in the C57BL/6 inbred strain. It has been reported that C57BL/6, FVB/NL and BALB/c mice (all inbred) are highly susceptible to systemic LPS challenge, while A/J, C3H/HeJ and 129S1/SvImJ mice (all inbred) are more resistant [29–31]. To our knowledge, no information is available in the literature on the susceptibility of outbred strains to LPS. In this study, a single LPS exposure induced neuroinflammation in the brain and initiated self-perpetuating mechanisms that persisted for at least 5 days in the inbred strain and 1 day in the outbred strain. CD1 outbred mice are generally used for genetics, toxicology, pharmacology, and ageing research, whereas C57BL/6 inbred mice are used for transgenic and knockout model development as well as for obesity and immunological studies. Outbred mice have more genetic diversity and are more robust than inbred mice. On the other hand, inbred mice are almost genetically identical, which allows easier interpretation of experiments and fewer deviations.

Our study did not consider the effects of different LPS doses nor multiple time points after LPS administration on mGluR5 and TSPO levels. However, both parameters are crucial for interpretation when neuroinflammatory effects are expected [32]. We can only speculate that mGluR5 and/or TSPO levels might be regulated in a dose-dependent manner. With respect to timing, we observed a decrease in mGluR5 (both mRNA and protein) and TSPO (mRNA) levels, which returned to baseline levels in CD1 but not in C57BL/6 mice

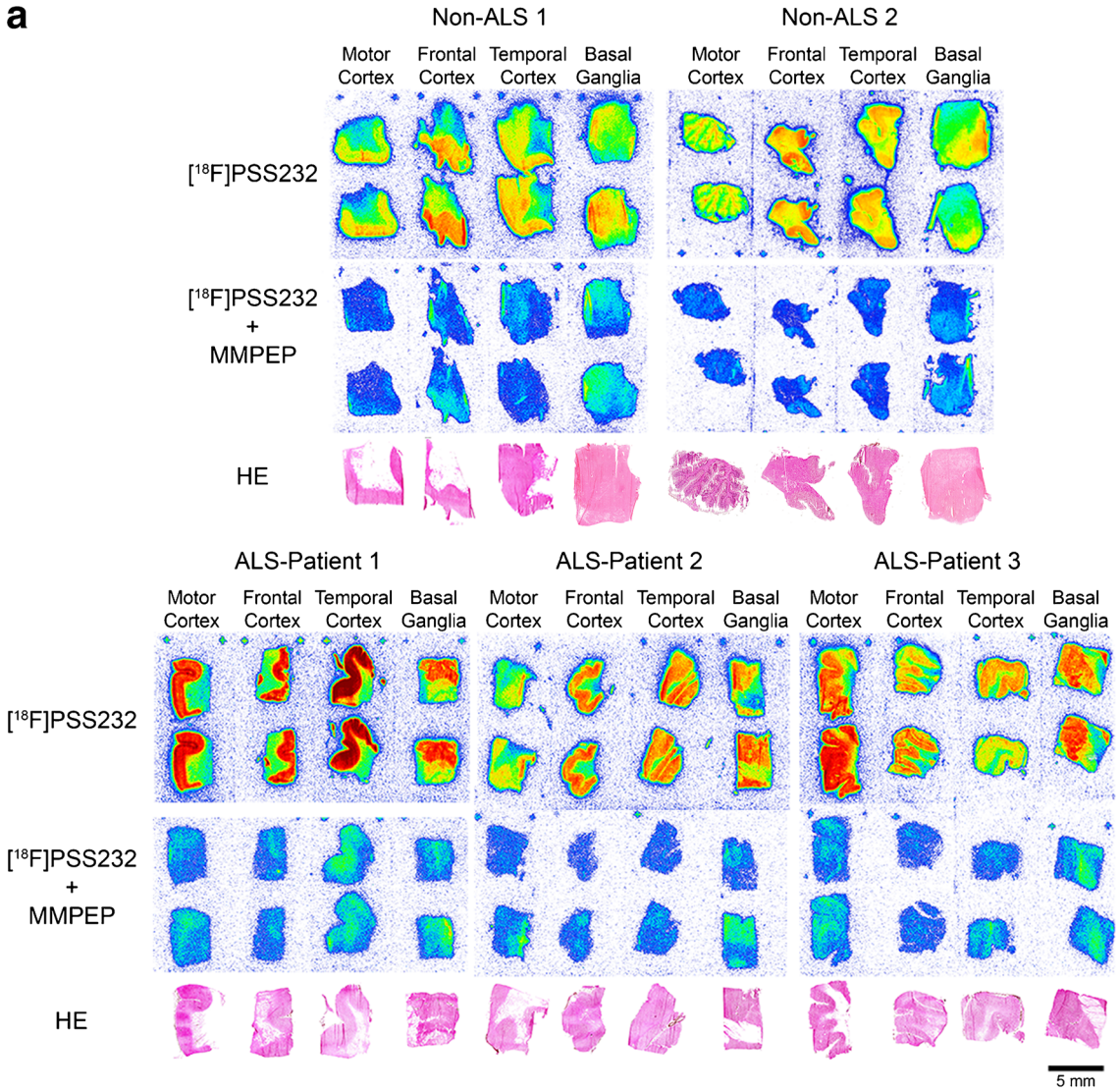
a
Non-ALS 1
Non-ALS 2
Motor Cortex
Frontal Cortex
Temporal Cortex
Basal Ganglia
[18F]PSS232
[18F]PSS232 + MMPEP
HE
ALS-Patient 1
ALS-Patient 2
ALS-Patient 3
5 mm

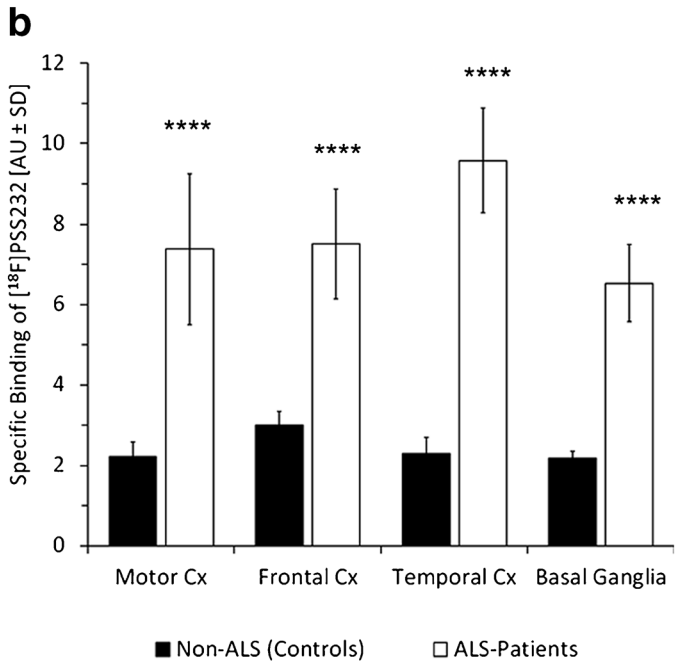
b
Specific Binding of [18F]PSS232 [AU ± SD]
12
10
8
6
4
2
0
****
Motor Cx
Frontal Cx
Temporal Cx
Basal Ganglia
Non-ALS (Controls)
ALS-Patients

◀ **Fig. 5** **a** In vitro autoradiography of [^{18}F]PSS232 (1 nM) in brains from non-ALS patients (control 1 and control 2) and ALS patients (patient 1 to patient 3) post mortem. Availability of mGluR5 is higher in the cortex and basal ganglia in ALS brains. Nondisplaceable binding was defined by incubation of replicate slices with 1 nM [^{18}F]PSS232 and 1 μM MMPEP. Tissue slices of cortical brain regions and basal ganglia stained with haematoxylin and eosin (HE) are also shown. **b** Quantitative autoradiography measurement for specific binding of [^{18}F]PSS232 in the cortex (*Cx*) and basal ganglia from three independent experiments with two tissue slices each (*AU* arbitrary units, *SD* standard deviation). ****$p < 0.0001$, non-ALS tissue versus ALS tissue

at 5 days after LPS administration. A follow-up study investigating later time points or time points between 1 and 5 days would be beneficial to further elucidate the process of mGluR5 regulation.

Peripherally-injected LPS induces a variety of central effects mediated by numerous factors. The results of previous studies on proinflammatory cytokines and receptors in the brain [5, 32] differ considerably possibly because of the contrasting methodological aspects of the reported experiments. The LPS strains used (*E. coli*, *Salmonella*), mouse strains used, age of the mice, site of injection (intraperitoneal, intrastriatal), doses of LPS administered and time after challenge could all be contributing factors. Our study did not investigate all these diverse experimental setups and our conclusions on the regulation of mGluR5 are limited to the setups described.

The in vitro autoradiography experiments using brain slices from patients with severe ALS and AD showed increased availability of mGluR5 specifically in the cortex, basal ganglia and hippocampus, but not in the cerebellum, at least in AD brains. The measured mGluR5 levels are valid only for the disease stage studied (severe, late) and cannot be assumed to be valid for early stages of ALS and AD or for stages of neuroinflammation in general (e.g. numbers of CD68-positive or TSPO-positive cells). Immunohistochemical staining verifying upregulated mGluR5 levels and correlating them with, for example, TSPO levels would strengthen the findings of the in vitro autoradiography. Another limitation was the low availability of human brain tissue from both early and late stage disease, which restricted the number of samples available for evaluation in this study. However, the fact that we observed threefold to fourfold higher mGluR5 levels in the cortex of ALS brains and fivefold higher levels in the cortex of AD brains compared with control brains suggests that if the number of control samples were increased we would still observe increases in mGluR5 levels in ALS and AD brains. Nevertheless, our autoradiography experiments confirmed our observations in the LPS-induced mouse model of neuroinflammation. In both cases, we demonstrated higher mGluR5 availability in brain regions that express mGluR5 at basal levels. In contrast, mGluR5 availability was not affected by neuroinflammation in brain regions with low mGluR5 levels such as the cerebellum.

It must be kept in mind that phenomena observed in mice may not necessarily occur in the same way in humans because of differences between mouse and human immune systems [33]. Nevertheless, in this study, neuroinflammation led to an increase in mGluR5 availability in both species. Other preclinical studies in ALS and AD animal models have shown mGluR5 upregulation in both diseases. A [^{18}F]FPEB PET imaging study showed enhanced levels of mGluR5 in an ALS mouse model expressing the SOD1-G93A gene [34]. Cortical astrocytes derived from rats carrying the human SOD1 gene (hSOD1^{G93A}) have also been found to show enhanced expression of functional mGluR5 in comparison with cells from wild-type rats [35]. In the amyloid-β peptide pathology mouse model tg-ArcSwe, mGluR5 levels were found on [^{11}C]ABP688 PET imaging to be higher than in wild-type mice [36]. However, in the 5xFAD AD mouse model levels mGluR5 were found on [^{18}F]FPEB PET imaging to be downregulated [37]. In line with our in vitro autoradiography results showing upregulated mGluR5 levels in ALS and AD brains, it has been shown that mGluR5 expression in ALS brains is increased in reactive glial cells with regional differences [38]. Another example is the ability of the amyloid-β peptide to actively interact with mGluR5, indicating a possible role of the receptor in neurodegeneration associated with proteinopathies [28]. Although the pathophysiological relevance of upregulated mGluR5 in reactive astrocytes and glial cells is unclear, it may represent a critical mechanism for modulation of glial function and changes in glial–neuronal communication in the course of neurodegeneration in ALS as well as in AD.

Besides the excitotoxicity and proinflammatory effects triggered by mGluR5, numerous studies have shown that activation of mGluR5 might lead to reductions in the number of reactive glial cells, and the amount of brain inflammation and neurotoxicity [12, 14, 39, 40]. These antiinflammatory properties are associated with a lower level of brain degeneration and a reduction in neurological deficits. This led to the hypothesis that glial cells behave differently depending on the type of stimuli and binding receptor [21].

The neuroprotective effects of downregulation or pharmacological blockade of mGluR5 emphasizes the potential of therapeutic interventions. The strategy of reducing inflammation in neurodegenerative disease has attracted increasing attention in recent years. Metabotropic glutamate receptor agonists, antagonists, ligands to allosteric sites (synthetic or natural compounds) are being tested in preclinical models as well as in clinical trials [41]. Genetic deletion of mGluR5 or its blockade by selective negative allosteric modulators (NAMs, e.g. MTEP) has been shown to reverse learning and memory deficits and rescue synapse loss in AD transgenic mice [42, 43]. More recently, the mGluR5-selective NAM, 2-chloro-

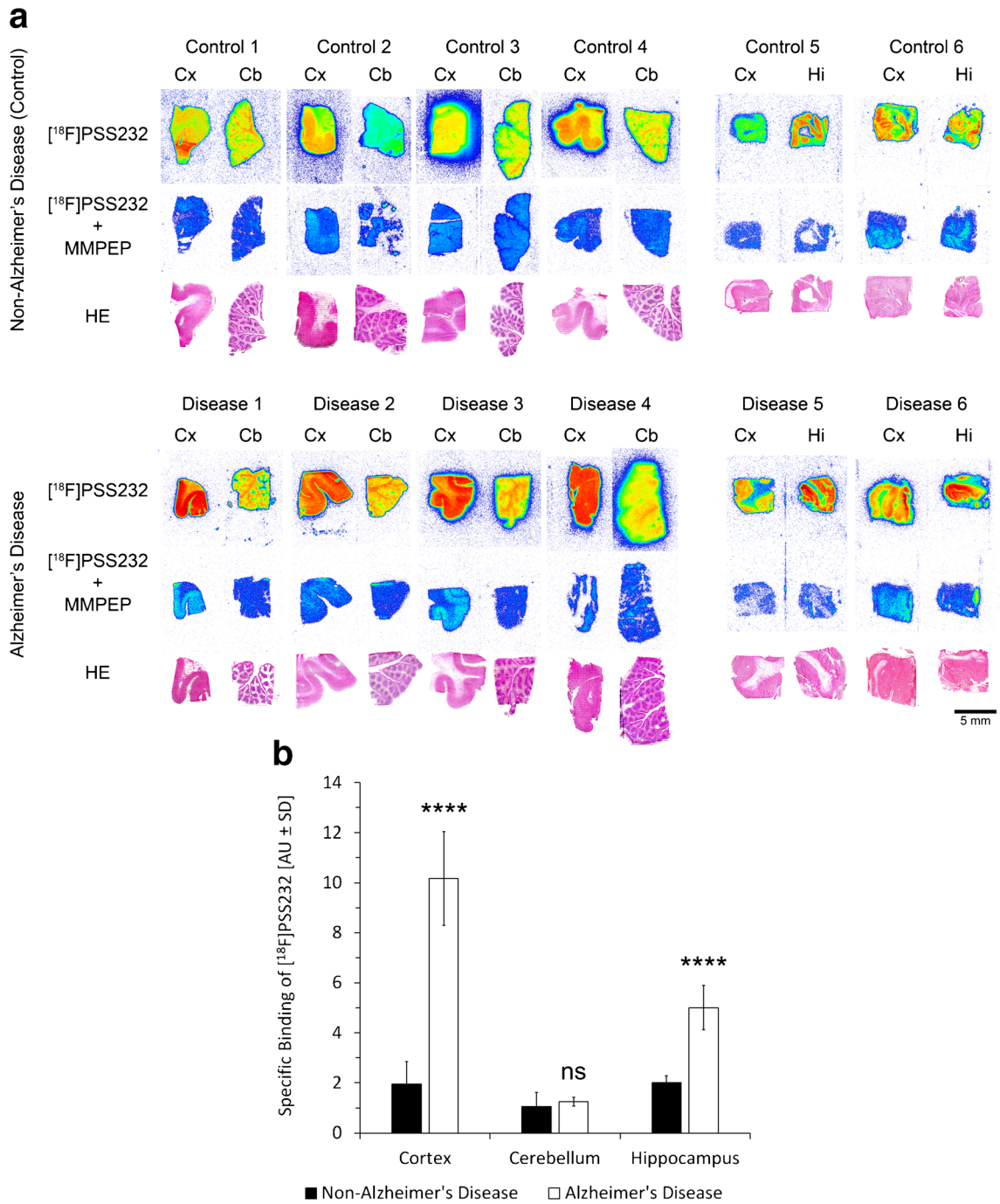

Fig. 6 In vitro mGluR5 autoradiography on human brain tissue from non-Alzheimer's disease patients (control 1 to control 6) and Alzheimer's disease patients (disease 1 to disease 6) post mortem. **a** Non-AD tissue shows moderate [^{18}F]PSS232 binding in the cortex, cerebellum and hippocampus. AD tissue shows strong [^{18}F]PSS232 binding in the cortex and hippocampus, but moderate binding in the cerebellum (*Cx* cortex, *Cb* cerebellum, *Hi* hippocampus). Nondisplaceable binding was defined by incubation of replicate slices with 1 nM [^{18}F]PSS232 and 1 μM MMPEP. Tissue slices stained with haematoxylin and eosin (HE) show tissue morphology. **b** Specific binding of [^{18}F]PSS232 determined by in vitro autoradiography in two independent experiments with two tissue slices each (*AU* arbitrary units, *SD* standard deviation). ****$p < 0.0001$, non-AD tissue versus AD tissue

4-[2-[2,5-dimethyl-1-[4-(trifluoromethoxy)phenyl]imidazol-4-yl]ethynyl]pyridine (CTEP), has been shown to improve cognitive performance and to reduce plaque pathology when chronically administered to AD transgenic mice [44]. From a therapeutic standpoint, it is noteworthy that neutral allosteric ligands (NALs, e.g. BMS-982423) spare normal mGluR5 signalling while reducing the pathological signal generated by mGluR5-containing receptor complexes [45]. Overall, the study of mGluR5 NALs or partial NAMs is among the most promising lines of preclinical AD research [41]. Future studies

are necessary and important to verify whether a therapeutic effect can be followed by imaging mGluR5.

In conclusion, our study demonstrates that noninvasive PET imaging using [^{18}F]PSS232 has the potential to evaluate mGluR5 availability in neuroinflammation-related diseases. Since our fluorinated mGluR5 PET radiotracer has already been evaluated in healthy volunteers, and exhibits well-defined kinetics with the possibility of using reference tissue models [46], it could easily be used in clinical PET imaging studies in patients with neurodegenerative disorders such as ALS and AD, and potentially also for therapy monitoring. Future clinical PET studies will show the utility of mGluR5 imaging in neurodegenerative brain diseases.

Acknowledgments We acknowledge Claudia Keller for LPS administrations and animal care and for performing the PET/CT scans. We thank Bruno Mancosu for [^{18}F]PSS232 production and Dr. Linjing Mu for her support in radiolabelling and quality control as well as for fruitful discussions. We thank Prof. Stefanie D. Krämer for rewarding discussions during the study. We acknowledge Dr. Markus Margelisch (Cantonal Hospital St. Gallen, Switzerland) for providing the human ALS brain tissue. We thank Prof. Julian Romero (University Hospital Alcorcón, Spain), Brain Bank (Hospital Universitario Fundación Alcorcón, Madrid, Spain) and Prof. Catriona McLean with Prof. Colin Masters (Victorian Brain Bank Network, Melbourne, Australia) for providing the Alzheimer's disease brain slices. We acknowledge the support of the Scientific Center for Optical and Electron Microscopy (ScopeM) of ETH Zurich.

Compliance with ethical standards

Conflicts of interest None.

Ethical approval All applicable international, national, and/or institutional guidelines for the care and use of animals were followed. All procedures performed in studies involving animals were in accordance with the ethical standards of the institution or practice at which the studies were conducted.

All procedures performed in studies involving human tissue were in accordance with the ethical standards of the institutional and/or national research committee and with the principles of the 1964 Declaration of Helsinki and its later amendments or comparable ethical standards.

References

1. Amor S, Puentes F, Baker D, van der Valk P. Inflammation in neurodegenerative diseases. Immunology. 2010;129:154–69. https://doi.org/10.1111/j.1365-2567.2009.03225.x.
2. Jellinger KA. Basic mechanisms of neurodegeneration: a critical update. J Cell Mol Med. 2010;14:457–87. https://doi.org/10.1111/j.1582-4934.2010.01010.x.
3. Tohidpour A, Morgun AV, Boitsova EB, Malinovskaya NA, Martynova GP, Khilazheva ED, et al. Neuroinflammation and infection: molecular mechanisms associated with dysfunction of neurovascular unit. Front Cell Infect Microbiol. 2017;7:276. https://doi.org/10.3389/fcimb.2017.00276.
4. Nazem A, Sankowski R, Bacher M, Al-Abed Y. Rodent models of neuroinflammation for Alzheimer's disease. J Neuroinflammation. 2015;12:74. https://doi.org/10.1186/s12974-015-0291-y.
5. Catorce MN, Gevorkian G. LPS-induced murine neuroinflammation model: main features and suitability for pre-clinical assessment of nutraceuticals. Curr Neuropharmacol. 2016;14:155–64.
6. Rubio-Perez JM, Morillas-Ruiz JM. A review: inflammatory process in Alzheimer's disease, role of cytokines. ScientificWorldJournal. 2012;2012:756357. https://doi.org/10.1100/2012/756357.
7. Nadeau S, Rivest S. Effects of circulating tumor necrosis factor on the neuronal activity and expression of the genes encoding the tumor necrosis factor receptors (p55 and p75) in the rat brain: a view from the blood-brain barrier. Neuroscience. 1999;93:1449–64.
8. Qin L, Wu X, Block ML, Liu Y, Breese GR, Hong JS, et al. Systemic LPS causes chronic neuroinflammation and progressive neurodegeneration. Glia. 2007;55:453–62. https://doi.org/10.1002/glia.20467.
9. Ifuku M, Katafuchi T, Mawatari S, Noda M, Miake K, Sugiyama M, et al. Anti-inflammatory/anti-amyloidogenic effects of plasmalogens in lipopolysaccharide-induced neuroinflammation in adult mice. J Neuroinflammation. 2012;9:197. https://doi.org/10.1186/1742-2094-9-197.
10. Sheng JG, Bora SH, Xu G, Borchelt DR, Price DL, Koliatsos VE. Lipopolysaccharide-induced-neuroinflammation increases intracellular accumulation of amyloid precursor protein and amyloid beta peptide in APPswe transgenic mice. Neurobiol Dis. 2003;14:133–45.
11. Crawshaw AA, Robertson NP. The role of TSPO PET in assessing neuroinflammation. J Neurol. 2017;264:1825–7. https://doi.org/10.1007/s00415-017-8565-1.
12. Drouin-Ouellet J, Brownell AL, Saint-Pierre M, Fasano C, Emond V, Trudeau LE, et al. Neuroinflammation is associated with changes in glial mGluR5 expression and the development of neonatal excitotoxic lesions. Glia. 2011;59:188–99. https://doi.org/10.1002/glia.21086.
13. Piers TM, Kim DH, Kim BC, Regan P, Whitcomb DJ, Cho K. Translational concepts of mGluR5 in synaptic diseases of the brain. Front Pharmacol. 2012;3:199. https://doi.org/10.3389/fphar.2012.00199.
14. Byrnes KR, Loane DJ, Stoica BA, Zhang J, Faden AI. Delayed mGluR5 activation limits neuroinflammation and neurodegeneration after traumatic brain injury. J Neuroinflammation. 2012;9:43. https://doi.org/10.1186/1742-2094-9-43.
15. Awad H, Hubert GW, Smith Y, Levey AI, Conn PJ. Activation of metabotropic glutamate receptor 5 has direct excitatory effects and potentiates NMDA receptor currents in neurons of the subthalamic nucleus. J Neurosci. 2000;20:7871–9.
16. Jong YJ, Kumar V, O'Malley KL. Intracellular metabotropic glutamate receptor 5 (mGluR5) activates signalling cascades distinct from cell surface counterparts. J Biol Chem. 2009;284:35827–38. https://doi.org/10.1074/jbc.M109.046276.
17. Abushik PA, Niittykoski M, Giniatullina R, Shakirzyanova A, Bart G, Fayuk D, et al. The role of NMDA and mGluR5 receptors in calcium mobilization and neurotoxicity of homocysteine in trigeminal and cortical neurons and glial cells. J Neurochem. 2014;129:264–74. https://doi.org/10.1111/jnc.12615.
18. Luyt K, Varadi A, Durant CF, Molnar E. Oligodendroglial metabotropic glutamate receptors are developmentally regulated and involved in the prevention of apoptosis. J Neurochem. 2006;99:641–56. https://doi.org/10.1111/j.1471-4159.2006.04103.x.
19. Milicevic Sephton S, Müller Herde A, Mu L, Keller C, Rudisuhli S, Auberson Y, et al. Preclinical evaluation and test-retest studies of [(18)F]PSS232, a novel radioligand for targeting metabotropic glutamate receptor 5 (mGlu5). Eur J Nucl Med Mol Imaging. 2015;42:128–37. https://doi.org/10.1007/s00259-014-2883-7.
20. Müller Herde A, Keller C, Milicevic Sephton S, Mu L, Schibli R, Ametamey SM, et al. Quantitative positron emission tomography of mGluR5 in rat brain with [(18) F]PSS232 at minimal invasiveness and reduced model complexity. J Neurochem. 2015;133:330–42. https://doi.org/10.1111/jnc.13001.

21. Arsenault D, Coulombe K, Zhu A, Gong C, Kil KE, Choi JK, et al. Loss of metabotropic glutamate receptor 5 function on peripheral benzodiazepine receptor in mice prenatally exposed to LPS. PLoS One. 2015;10:e0142093. https://doi.org/10.1371/journal.pone.0142093.
22. Ametamey SM, Treyer V, Streffer J, Wyss MT, Schmidt M, Blagoev M, et al. Human PET studies of metabotropic glutamate receptor subtype 5 with 11C-ABP688. J Nucl Med. 2007;48:247–52.
23. Ferraguti F, Corti C, Valerio E, Mion S, Xuereb J. Activated astrocytes in areas of kainate-induced neuronal injury upregulate the expression of the metabotropic glutamate receptors 2/3 and 5. Exp Brain Res. 2001;137:1–11.
24. D'Ascenzo M, Fellin T, Terunuma M, Revilla-Sanchez R, Meaney DF, Auberson YP, et al. mGluR5 stimulates gliotransmission in the nucleus accumbens. Proc Natl Acad Sci U S A. 2007;104:1995–2000. https://doi.org/10.1073/pnas.0609408104.
25. Pin JP, Duvoisin R. The metabotropic glutamate receptors: structure and functions. Neuropharmacology. 1995;34:1–26.
26. Endoh T. Characterization of modulatory effects of postsynaptic metabotropic glutamate receptors on calcium currents in rat nucleus tractus solitarius. Brain Res. 2004;1024:212–24. https://doi.org/10.1016/j.brainres.2004.07.074.
27. Mannaioni G, Marino MJ, Valenti O, Traynelis SF, Conn PJ. Metabotropic glutamate receptors 1 and 5 differentially regulate CA1 pyramidal cell function. J Neurosci. 2001;21:5925–34.
28. Kumar A, Dhull DK, Mishra PS. Therapeutic potential of mGluR5 targeting in Alzheimer's disease. Front Neurosci. 2015;9:215. https://doi.org/10.3389/fnins.2015.00215.
29. De Maio A, Mooney ML, Matesic LE, Paidas CN, Reeves RH. Genetic component in the inflammatory response induced by bacterial lipopolysaccharide. Shock. 1998;10:319–23.
30. Hopkins W, Gendron-Fitzpatrick A, McCarthy DO, Haine JE, Uehling DT. Lipopolysaccharide-responder and nonresponder C3H mouse strains are equally susceptible to an induced Escherichia coli urinary tract infection. Infect Immun. 1996;64:1369–72.
31. Yang IV, Rutledge HR, Yang J, Warg LA, Sevilla SD, Schwartz DA. A locus on chromosome 9 is associated with differential response of 129S1/SvImJ and FVB/NJ strains of mice to systemic LPS. Mamm Genome. 2011;22:518–29. https://doi.org/10.1007/s00335-011-9340-8.
32. Lopes PC. LPS and neuroinflammation: a matter of timing. Inflammopharmacology. 2016;24:291–3. https://doi.org/10.1007/s10787-016-0283-2.
33. Mestas J, Hughes CC. Of mice and not men: differences between mouse and human immunology. J Immunol. 2004;172:2731–8.
34. Brownell AL, Kuruppu D, Kil KE, Jokivarsi K, Poutiainen P, Zhu A, et al. PET imaging studies show enhanced expression of mGluR5 and inflammatory response during progressive degeneration in ALS mouse model expressing SOD1-G93A gene. J Neuroinflammation. 2015;12:217. https://doi.org/10.1186/s12974-015-0439-9.
35. Vermeiren C, Hemptinne I, Vanhoutte N, Tilleux S, Maloteaux JM, Hermans E. Loss of metabotropic glutamate receptor-mediated regulation of glutamate transport in chemically activated astrocytes in a rat model of amyotrophic lateral sclerosis. J Neurochem. 2006;96:719–31. https://doi.org/10.1111/j.1471-4159.2005.03577.x.
36. Fang XT, Eriksson J, Antoni G, Yngve U, Cato L, Lannfelt L, et al. Brain mGluR5 in mice with amyloid beta pathology studied with in vivo [(11)C]ABP688 PET imaging and ex vivo immunoblotting. Neuropharmacology. 2017;113:293–300. https://doi.org/10.1016/j.neuropharm.2016.10.009.
37. Lee M, Lee HJ, Park IS, Park JA, Kwon YJ, Ryu YH, et al. Abeta pathology downregulates brain mGluR5 density in a mouse model of Alzheimer. Neuropharmacology. 2018;133:512–7. https://doi.org/10.1016/j.neuropharm.2018.02.003.
38. Lee HG, Zhu X, O'Neill MJ, Webber K, Casadesus G, Marlatt M, et al. The role of metabotropic glutamate receptors in Alzheimer's disease. Acta Neurobiol Exp (Wars). 2004;64:89–98.
39. Byrnes KR, Stoica B, Loane DJ, Riccio A, Davis MI, Faden AI. Metabotropic glutamate receptor 5 activation inhibits microglial associated inflammation and neurotoxicity. Glia. 2009;57:550–60. https://doi.org/10.1002/glia.20783.
40. Loane DJ, Stoica BA, Pajoohesh-Ganji A, Byrnes KR, Faden AI. Activation of metabotropic glutamate receptor 5 modulates microglial reactivity and neurotoxicity by inhibiting NADPH oxidase. J Biol Chem. 2009;284:15629–39. https://doi.org/10.1074/jbc.M806139200.
41. Caraci F, Nicoletti F, Copani A. Metabotropic glutamate receptors: the potential for therapeutic applications in Alzheimer's disease. Curr Opin Pharmacol. 2018;38:1–7. https://doi.org/10.1016/j.coph.2017.12.001.
42. Haas LT, Kostylev MA, Strittmatter SM. Therapeutic molecules and endogenous ligands regulate the interaction between brain cellular prion protein (PrPC) and metabotropic glutamate receptor 5 (mGluR5). J Biol Chem. 2014;289:28460–77. https://doi.org/10.1074/jbc.M114.584342.
43. Hamilton A, Esseltine JL, DeVries RA, Cregan SP, Ferguson SS. Metabotropic glutamate receptor 5 knockout reduces cognitive impairment and pathogenesis in a mouse model of Alzheimer's disease. Mol Brain. 2014;7:40. https://doi.org/10.1186/1756-6606-7-40.
44. Hamilton A, Vasefi M, Vander Tuin C, McQuaid RJ, Anisman H, Ferguson SS. Chronic pharmacological mGluR5 inhibition prevents cognitive impairment and reduces pathogenesis in an Alzheimer disease mouse model. Cell Rep. 2016;15:1859–65. https://doi.org/10.1016/j.celrep.2016.04.077.
45. Haas LT, Salazar SV, Smith LM, Zhao HR, Cox TO, Herber CS, et al. Silent allosteric modulation of mGluR5 maintains glutamate signalling while rescuing Alzheimer's mouse phenotypes. Cell Rep. 2017;20:76–88. https://doi.org/10.1016/j.celrep.2017.06.023.
46. Warnock G, Sommerauer M, Mu L, Pla Gonzalez G, Geistlich S, Treyer V, et al. A first-in-man PET study of [(18)F]PSS232, a fluorinated ABP688 derivative for imaging metabotropic glutamate receptor subtype 5. Eur J Nucl Med Mol Imaging. 2018;45:1041–51. https://doi.org/10.1007/s00259-017-3879-x.